Structural, dielectric and electrical properties of $Li_2Pb_2La_2W_2Ti_4Nb_4O_{30}$ ceramic

B N PARIDA, PIYUSH R DAS*, R PADHEE and R N P CHOUDHARY

Department of Physics, Institute of Technical Education and Research, Siksha 'O' Anusandhan University, Bhubaneswar 751 030, India

Abstract. $Li_2Pb_2La_2W_2Ti_4Nb_4O_{30}$ complex ferroelectric oxide was prepared by using a high-temperature solid-state reaction method (calcination temperature, ∼1100 °C and sintering temperature, ∼1150 °C). Room temperature preliminary structural analysis shows formation of a single-phase compound. The nature of microstructure (i.e. grain distribution, presence of voids, grain size, etc) recorded using scanning electron microscope (SEM) clearly suggests the formation of high quality and density of pellet samples. Studies of temperature dependence of dielectric constant, tangent loss and polarization show the existence of ferroelectric phase transition in the material at high temperature (307 °C). Detailed studies of temperature dependence of electrical parameters (i.e. impedance (400−475 °C), modulus, conductivity, etc) of the material clearly suggest a strong correlation between its microstructure (i.e. bulk, grain boundary, etc) and electrical properties. The nature of temperature variation of d.c. conductivity showed an Arrhenius behaviour of the material. A signature of ionic conductivity in the material was observed in its a.c. conductivity spectrum. The nature of frequency dependence of a.c. conductivity of the material can be explained by Jonscher's universal power law. Electrical transport properties of the material show existence of non-exponential type of conductivity relaxation.

Keywords. Solid-state reaction; X-ray methods; ferroelectric properties; impedance; electrical conductivity.

1. Introduction

After the first report of nonlinearity in dielectric and polarization properties in an oxide compound, $BaTiO_3$ (Wul and Goldman 1945), a large number of oxides of similar and/or different structural family were examined in search of new oxide materials for device applications. Among all the ferroelectric oxides known today, some oxides of perovskite and tungsten–bronze (TB) structural families have been found more fascinating and useful for piezoelectric, pyroelectric and ferroelectric memory devices at room temperature, (Choudhary *et al* 1999; Sahoo *et al* 2010). The compounds of perovskite structural family of a general formula, ABO_3 (A = mono-divalent ions, B = tri-hexavalent ions) type, have simple and ordered structure, whereas those of tungsten–bronze structural family can be regarded (as being a derivative of classical perovskite ABO_3) complex and disordered in which, the BO_3 framework is transformed to create *A* sites interstices larger than cuboctahedron. Hence, the structure can be described as an array of distorted octahedral sharing corners in such a way that, three different types of interstices *A*, *B* and *C* are available for cation substitution with a general formula, $[(A_1)_2(A_2)_4](C)_4[(B_1)_2(B_2)_8]O_{30}$. A_1 cavities have cuboctahedral coordination of oxygen atoms; A_2 cavities have a pentagonal prismatic coordination and *C* sites have a trigonal prismatic one. B_1 and B_2 sites are substituted with octahedral coordination. Size of these cavities decreases in the order of $A_2 > A_1 > C$ (Muktha *et al* 2006). In a typical TB structure, *A*-site is occupied by mono to trivalent cations, *B*-sites are occupied by tetrahexavalent ions and *C*-site is either unfilled or occupied by small ions, having complex and disordered structure. Size and type of substituted ions or atoms at different sites and amount of disorder have a significant effect on dielectric and ferroelectric properties of the material. Because of the simplicity and stability of the perovskite structure, it is easy to understand physics of the materials. Whereas, it is more difficult for the materials of TB structural family. However, the complexity of TB structure has provided many interesting and varieties of physical properties useful for applications. As TB is a complex system, suitable modifications at different sites can be made in order to tailor the physical properties or device parameters of the materials as required for a particular application.

Since the discovery of ferroelectric properties in a tungsten–bronze compound (Goodman 1953), a large number of compounds of TB family have been prepared and investigated in different forms (i.e. single crystal, ceramics and thin films) keeping in mind the possible applications. Structural, ferroelectric and electrical transport properties of some compounds related to this paper such as $Pb_3R_3Ti_5Nb_5O_{30}$ (R = rare-earth ion) have already been reported earlier (Goodman 1953; Hornebecq *et al* 2000; Behera *et al* 2005; Fang *et al* 2005; Kim *et al* 2006; Muktha *et al* 2006). The ferroelectric and related properties

---

in multi-valence complex tungsten–bronze structure have been reported (Smolenskii and Agranovskaya 1954), not much work has been done on any of the compounds having all six valences. In order to tailor the physical properties and ferroelectric transition temperature in such type of compounds, many compounds including $Na_2Pb_2Sm_2W_2Ti_4Nb_4O_{30}$ (Das *et al* 2007a, b, c), $Na_2Pb_2Nd_2W_2Ti_4Nb_4O_{30}$ (Das *et al* 2008) and $Na_2Pb_2R_2W_2Ti_4V_4O_{30}$ (R = Gd, Eu) have been studied earlier (Das *et al* 2007a, b, c). In our previously reported compounds (Das *et al* 2007a, b, c, 2008), we have low transition temperature as well as low loss as compared to the presently studied compound. The dielectric constant of the above compounds is significantly low for device applications. Again, degree of disorder of previously reported compounds is more than that of present compound. More recently, structural, dielectric and electrical properties of $CaBa_4SmTi_3Nb_7O_{30}$ (Ganguli and Jha 2011), dielectric and pyroelectric properties of $Ba_5SmTi_3Nb_7O_{30}$ (Ganguli *et al* 2009) have been reported. In the above compounds, we have observed low transition temperature as well as low tangent loss as compared to the presently studied compound. Once again, the degree of disorder (calculated from modified Curie–Weiss law) is more than that of present compound. The temperature variation of polarization was not studied in the above reported compounds, which has been included in our study to strengthen ferroelectricity in the compounds. There is no such variation in structure but transition temperature and dielectric constant increases significantly with the substitution of Li_2 in place of Na_2 and Nb_4 in place of V_4. Most recently, ferroelectric and related properties of $Li_2Pb_2Pr_2W_2Ti_4Nb_4O_{30}$ (LPPWTN) (Parida *et al* 2012) have been reported. Dielectric constant and tangent loss at T_c and diffusivity are relatively higher than that of other TB compounds. The value of $2P_r$ and $2E_c$ decreases with rise in temperature to verify the ferroelectricity in the above compound (LPPWTN), but conduction mechanism is both due to short- and long-range motions of charge carriers. Though a lot of work has been done, no work has been reported on the ferroelectric and related properties in $Li_2Pb_2La_2W_2Ti_4Nb_4O_{30}$ (LPLWTN) complex system, so we have completed them and reported here.

2. Experimental

The polycrystalline compound, $Li_2Pb_2La_2W_2Ti_4Nb_4O_{30}$ (LPLWTN), was synthesized by a high temperature solid-state reaction technique, using high-purity (AR grade) carbonate and oxides: Li_2CO_3, TiO_2, Nb_2O_5 and WO_3 (99%, M/s LOBA Chemie Pvt. Ltd., India), PbO (99.9%, M/s E Merk India Ltd.) and La_2O_3 (99.9%, M/s Indian rare-earth Ltd.). The oxides and carbonates were mixed in dry (air) and wet (methanol) medium for several hours in an agate mortar. The calcination was performed at temperature 1100 °C for 18 h. X-ray diffraction (XRD) data on calcined powder were recorded at room temperature using X-ray powder diffractometer (Rigaku Miniflex) with wavelength

$\lambda = 1.5405$ Å in a wide range of Bragg's angle (θ) ($20° \leq 2\theta \leq 80°$) at a scanning rate of 3 deg/min. The calcined powder mixed with polyvinyl alcohol (PVA) of the material was then cold pressed into cylindrical pellets of diameter, 12 mm and thickness, 1–2 mm at a pressure of 4×10^6 Nm^{-2} by using a hydraulic press. The pellets were then sintered at a temperature of 1150 °C for 4 h in air atmosphere. The sintered pellets were polished and coated with high-quality silver paste and dried at 160 °C for 8 h before taking any electrical measurements. The surface micrograph of the pellet sample was recorded by JEOL JSM_5800 scanning electron microscope (SEM). The dielectric (capacitance and dissipation factor), impedance and inductance parameters of silver-electroded pellet were measured as a function of frequency (1 kHz–1 MHz) at different temperatures (25–500 °C) using a computer-controlled impedance meter (PSM/4NL Model: 1735, UK). A chromel–alumel thermocouple and KUSAM MECO 108 digital millivoltmeter were used to record the temperatures. The hysteresis loops of the material were obtained on the poled sample (electric field = 12 kV/cm, time = 8 h) at different temperatures using a hysteresis loop tracer (M/s Marine India, New Delhi). Because of the experimental limitations on temperature, we could not record hysteresis loop above 200 °C to determine phase transition temperature as observed in our dielectric study. However, decreasing trend in the value of (a) remnant polarization, (b) saturated polarization and (c) area of the loops on increasing temperature confirms the existence of ferroelectric properties in the material below the transition temperature.

3. Results and discussion

3.1 *Structural analysis*

Figure 1 shows X-ray diffraction (XRD) pattern and SEM micrographs (inset) of LPLWTN recorded at room temperature on calcined powder and gold-coated pellet samples, respectively. As XRD pattern consists of sharp and single characteristic peaks (which is different from those of the ingredients of prepared compound), it exhibits better homogeneity and crystallization and the formation of single-phase new compound (Klug and Alexander 1974) is confirmed. Most of the peaks were indexed in an orthorhombic crystal system with different unit cell configurations using a standard computer program package 'POWD'. However, very small peaks with intensity close to the background of the pattern could not be indexed in the above systems and selected cell configuration. The lattice parameters (a, b and c) of a selected unit cell were refined using least-squares refinement sub-routine of POWD. The refined lattice parameters of the material are found to be: $a = 15.4116(20)$ Å, $b = 14.1192(20)$ Å, $c = 8.4016(20)$ Å and volume $V = 1828.18$ Å^3 (the number indicated in parenthesis is estimated error (standard deviation) in unit cell parameters). These parameters are very much consistent with those of reported
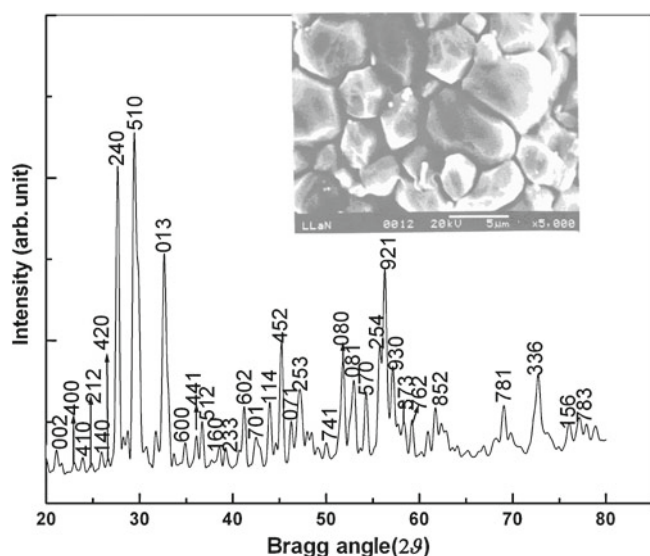
Figure 1. Indexed XRD and SEM patterns of LPLWTN.

Figure 2. Variation of relative dielectric constant with temperature as well as tangent loss with temperature of LPLWTN.

compounds of similar structure (Parida *et al* 2012). The orthorhombic distortion is given by $\delta = [b - a/b + a]$ which is 0·0438. Furthermore, TB structure is built on five crystallographic sites. It is difficult to precisely determine La^{+3} ions coordination (12- or 15-fold coordination) based on the current results. However, numerous structural studies show that rare-earth cations predominately prefer A_1-tunnels (Bouziane *et al* 2011).

Further, the scattered crystallite or particle size (P) of the compound was calculated using the broadening of some widely spread (over Bragg angles) strong and medium reflections in Scherrer's equation (Cullity 1978):

$$P_{hkl} = \frac{K\lambda}{\beta_{1/2} \cos \theta_{hkl}},$$

where K (constant) = 0·89, $\lambda = 1\cdot5405$ Å and $\beta_{1/2}$ = full width at half maximum (in radians). The average value of P is found to be 12 nm.

Figure 1 (inset) shows room temperature SEM surface micrograph of LPLWTN. Nature, size and distribution of grains in the micrograph suggest that the grain growth during sintering has been completed, and hence presence of secondary phase is not seen. In spite of sintering at optimized (high) temperature some voids of irregular shape and dimension are seen. Some small size grains are homogenously distributed throughout surface of the sample. Generally, most of the grains have rectangular shape and size dimension of 3–7 μm.

3.2 *Dielectric study*

The temperature and frequency dependence of ε_r (relative dielectric constant) and tan δ (tangent loss) is shown in figure 2. The value of ε_r increases on rise in temperature up
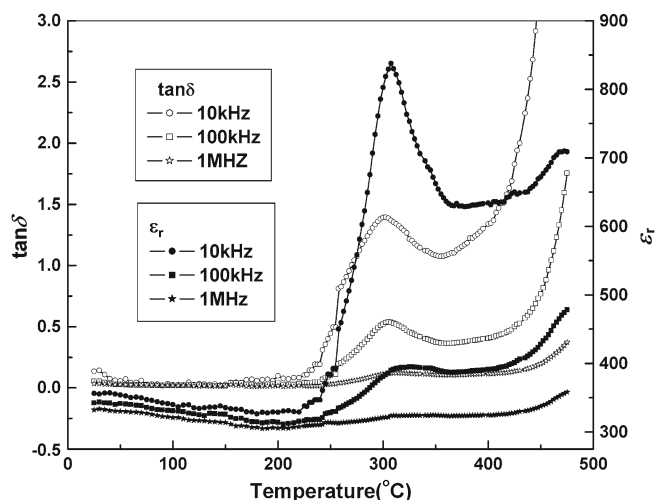
to a temperature (referred to as transition temperature (T_c)) and then decreases giving a dielectric anomaly. The variation in tan δ with temperature follows similar trend as of relative dielectric constant. In LPLWTN material, transition temperature, room temperature, dielectric constant and tangent loss of the materials are found to be 307, 356 and 0·056 °C, respectively. As the value of ε_{max} (dielectric constant, T_c) at 10, 100 and 1000 kHz is found to be 838, 394 and 328, respectively, and is frequency independent and the material is non-relaxor (Das *et al* 2008). The value of tan δ_{max} (tangent loss at T_c) at the above frequency is found to be 1·4, 0·55 and 0·12, respectively. The substitution of La at Pr-site in the compound reduces the transition temperature, this is due to decrease in the size of rare-earth ion. A large number of researchers have shown that T_c of lead-free lanthanide compounds decreases on increasing ionic radius of rare-earth cation. Josse *et al* (2009) reported that substitution of R^{+3} in A_1-tunnels induces distortions in the anionic framework. The smaller R^{+3} ions produce a greater distortion favouring an increase of T_c. In contrast, in lead-based TB compositions, the inverse effect can be observed (Sambasiva Rao *et al* 2008). As compared to LPPWTN (Parida *et al* 2012), studied material has low transition temperature, high room temperature dielectric constant and small and similar tangent loss. Initially tan δ is almost independent of temperature, whereas it is strongly dependent on temperature at higher temperatures. The sharp increase in tan δ at higher temperatures may be due to creation of large number of charge carriers and defects in the sample. Thus, at higher temperatures the conductivity begins to dominate, which is one of the reasons for rise in tan δ. Value of ε_{max} and tan δ_{max} of the titled compound decreases with rise in the frequency. Such a characteristic is normally found in normal ferroelectric material. A clear dispersion in tan δ at higher temperatures side can be seen in figure 2. A dielectric anomaly observed in figure 2 in the titled compound is assumed to be related to

the ferroelectric–paraelectric phase transition. This assumption has later been confirmed by observation of hysteresis loops at different temperatures (below T_c).

The dielectric peaks observed at different frequencies were found to be broadened or diffused, which is an indication of disordering in the material. In order to estimate the degree of diffuseness of dielectric peaks of the compound, a general expression (Pilgrim *et al* 1990):

$$\frac{1}{\varepsilon_r} - \frac{1}{\varepsilon_{max}} \alpha \ (T - T_c)^\gamma,$$

or

$$\ln\left(\frac{1}{\varepsilon_r} - \frac{1}{\varepsilon_{max}}\right) = \gamma \ln\left(T - T_c\right) + \text{constant},$$

is generally used, where symbols have their usual meanings. The diffusivity (γ), calculated from the slope of $\ln(1/\varepsilon_r - 1/\varepsilon_{max})$ vs $\ln(T - T_c)$ plots (using the linear portion of the graph as shown in figure 3), was found to be close to unity (1·06) suggesting to follow Curie–Weiss law. The substitution of La at Pr-site in the compound results in the reduction of diffusivity (γ) indicating an increase in ordering of the system (Ganguli *et al* 2009). Unlike the title compound, diffused phase transitions in many other TB structured ferroelectrics have been observed, which can support the presence of certain non-equivalent position in the unit cell (Parida *et al* 2012) of the compounds.

3.3 *Polarization study*

Figure 4 shows hysteresis loop of LPLWTN at three different temperatures. The value of remnant polarization (2Pr) of the compound at 50, 100 and 150 °C was found to be 9·83, 7·77, 5·22 μC/cm^2, respectively, whereas that of coercive field (E_c) at these temperatures was found to be 0·202,
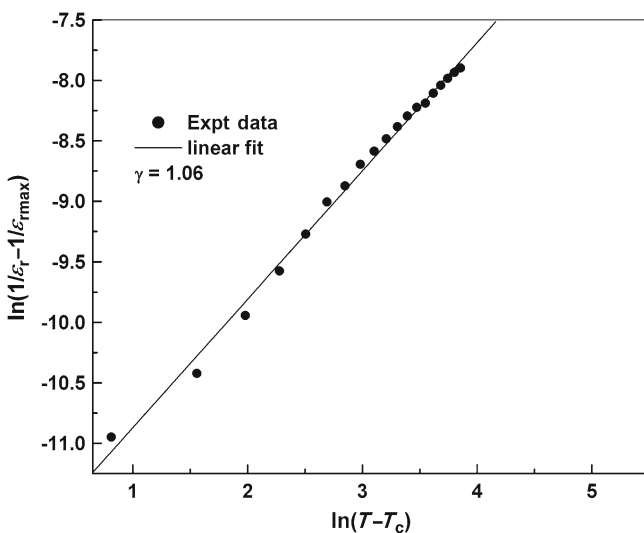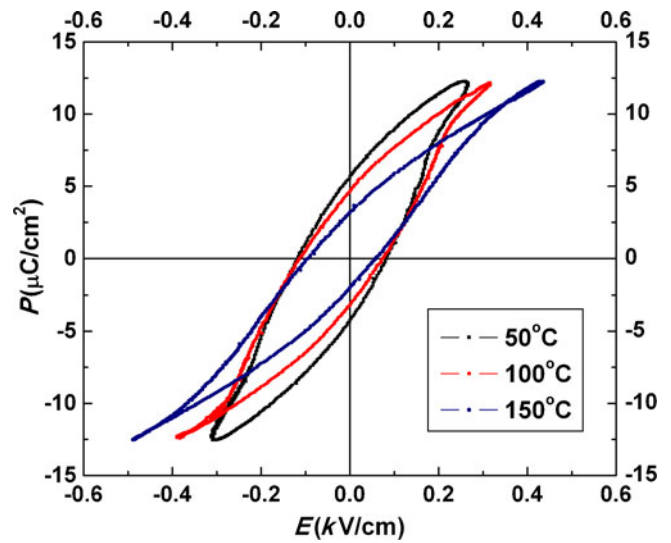

Figure 4. Hysteresis loop of LPLWTN at different temperatures.

0·185, 0·154 kV/cm, respectively. It is clear that LPLWTN compound has low coercive field and small remnant polarization, which are consistent with most of the complex ferroelectrics belonging to tungsten–bronze structural family. Again, decreasing trend of the above hysteresis loop parameters and area of the room temperature loop, with rise in temperature clearly suggest the existence of ferroelectric properties of the material. As compared to our previous work, this material has significantly higher remnant polarization and low coercive field implies material is loose.

3.4 *Impedance and modulus spectroscopy*

Nowadays, it is a well-established fact that complex impedance spectroscopy (CIS) is a non-destructive but powerful technique to characterize ferroelectrics and ionic materials at different frequencies and temperatures. This technique can be used to separate the contributions of (i) bulk, (ii) grain boundary and (iii) electrode polarization effect in the complex electrical properties of the material. An a.c. signal is applied across an electrode-pellet sample and its output response is measured. Measurements of impedance and related electrical parameters of a material give us the data having both real (resistive) and imaginary (reactive) components. For the analysis of experimental data, we have used some basic equations:

Complex impedance, $Z(\omega) = Z' + jZ''$,

complex modulus, $M(\omega) = \dfrac{1}{\varepsilon(\omega)} = M' + jM''$,
$$= j\omega C_0 Z,$$

complex admittance, $Y^* = Y' + jY'' = j\omega C_0 \varepsilon^*$
$$= (R_P)^{-1} + j\omega C_p,$$

Figure 3. $\ln\left(\frac{1}{\varepsilon_r} - \frac{1}{\varepsilon_{max}}\right) \sim \ln\left(T - T_c\right)$.

and

complex permittivity, $\varepsilon^* = \varepsilon' + j\varepsilon''$,

where $\omega = 2\pi f$ is the angular frequency; C_0 the geometrical capacitance, $j = \sqrt{-1}$, p and s refer to the parallel and series circuit components, respectively.

Peak of high frequency semicircular arcs of the complex impedance spectra enables us to calculate the relaxation frequency (ω_{max}) of the bulk material using the equation:

$$\omega_{max}\tau = \omega_{max}R_bC_b = 1 \Rightarrow 2\pi f_{max}R_bC_b,$$

where R_b is the bulk resistance and C_b the bulk capacitance.

3.4a *Impedance analysis*: Figure 5(a) shows variation of Z' with Z'' (usually referred to as Nyquist plot) at selected temperatures of LPLWTN over a wide range of frequency (1 kHz–1 MHz). The impedance is characterized by the appearance of temperature-dependent semicircular arcs. At lower temperatures, complex impedance plots show single semicircular arc (not shown here). At higher temperatures ($>350\,°C$), two semicircular arcs (with centre below the real axis) are observed. Most appropriate approach to interpret the depression of semicircles is statistical distribution of relaxation time (Nobre and Lanfredi 2003). The nature of

Figure 5. (**a**, **b**) Variation of Z' with Z'' of LPLWTN.

plots suggests that the electrical response consists of at least two semicircles; first due to bulk (grain) property of the material, whereas the second one (at higher temperatures) is due to contributions of grain boundary (Das *et al* 2007a, b).

Figure 5(a) (inset) shows comparison of experimental and fitted impedance data using commercially available software (ZSIMP WIN version 2.0). In Debye-like response, an equivalent circuit consists of a series combinations of (CQR) and (CR), where Q is known as constant phase element (CPE). The admittance of CPE is defined as
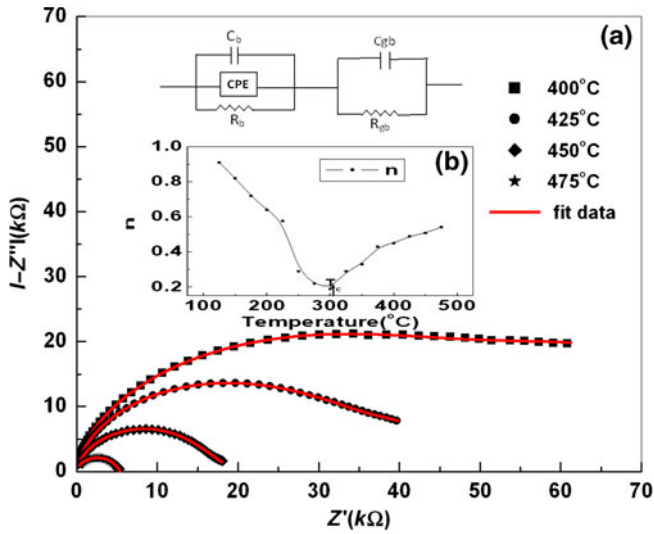
$$Y(CPE) = A_0(j\omega)^n = A\omega^n + jB\omega^n,$$

with

$$A = A_0\cos(n\pi/2) \text{ and } B = A_0\sin(n\pi/2),$$

where A_0 and n are frequency-independent but temperature-dependent parameters. A_0 the magnitude of dispersion and n value lies in between $0 \leq n \leq 1$ (for an ideal capacitor, $n = 1$ and for an ideal resistor, $n = 0$) (Macdonald 1984). The temperature variation of n is shown in figure 5(b). The value of n decreases and attain minimum nearby T_c, because of the absence of one of the transverse (soft) modes, restoring force tends to zero at ferroelectric–paraelectric phase transition (Lu *et al* 1992a, b). If charge carrier is coupled with soft mode, it becomes mobile near phase transition. From this fitted curves, the values of R_b (bulk resistance), R_{gb} (grain boundary resistance), bulk capacitance (C_b) and grain boundary capacitance (C_{gb}) at different temperatures were calculated and compared (table 1). It clearly shows that parameters R_b, R_{gb} and C_b decrease with rise in temperature implying the existence of negative temperature coefficient of resistance (NTCR) in the material (Ranjan *et al* 2011). The value of C_{gb} increases with rise in temperature because of the absence of interfacial effect (Suman *et al* 2006).

Figure 6 shows variation of Z' and Z'' as a function of frequency at some selected temperatures. The value of Z' decreases with rise in frequency and temperature which is related to electrical conductivity of the material. At high frequency, the value of Z' of each temperature coincides implying the possible release of space charge (Plocharski and Wieczoreck 1988; Sinclair and West 1989; Behera *et al* 2007; Sen *et al* 2007).
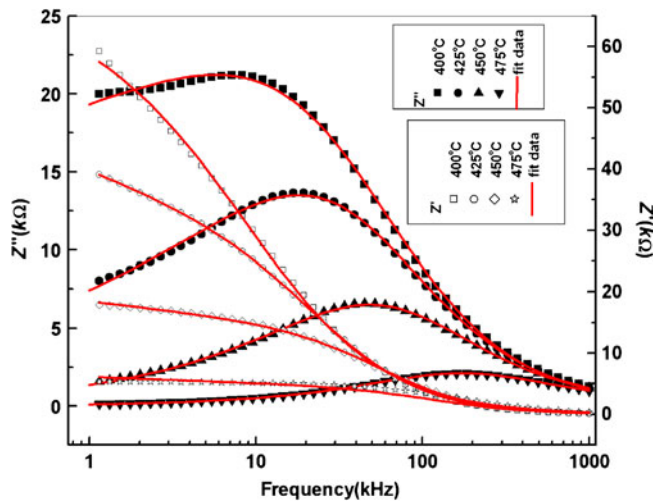
It is observed that at higher temperatures, the value of Z'' increases with rise in frequency to a maximum value (Z''_{max}) and then decreases. This suggests the presence of relaxation

Table 1. Comparison of bulk (grain) and grain boundary resistance and capacitance at different temperatures.

Temperature (°C)	R_b (kΩ)	C_b (nF)	R_{gb} (kΩ)	C_{gb} (nF)	CPE (nF)
350	253·8	0·1205	82·28	0·3378	457
375	105·8	0·1191	26·1	11·99	120·9
400	75·21	0·118	15·77	15·48	9·24
425	43·95	0·1157	5·07	42·78	577
450	15·76	0·1364	4·051	92·19	2168
475	4·512	0·1238	0·945	143·7	4837

Figure 6. Variation of Z' and Z'' with frequency at different temperatures of LPLWTN.

Figure 7. (**a**, **b**) Variation of fitting parameter m, n, f_1 and f_2 with temperature of LPLWTN.

in the sample (Behera *et al* 2008). Broadening of Z''_{max} peak with increase in temperature is a clear indication of the occurrence of temperature dependence of relaxation phenomenon in the material. The relaxation process occurs due to the presence of immobile charges at low temperatures, inherent defects and vacancies created during higher temperature processing of the sample (Jonscher 1977; Suman *et al* 2006).
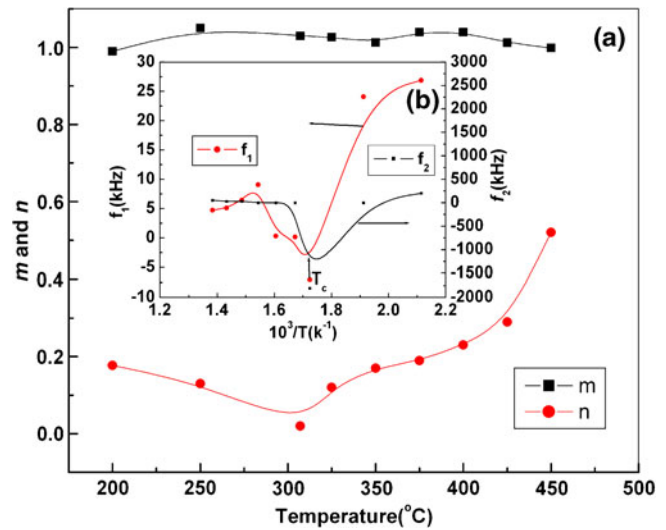
Again imaginary part of the impedance plot indicating high frequency slopes are independent of temperature. On the other hand, low frequency slopes are strongly temperature-dependent. Two temperature-dependent slopes suggest that there are two distinct dispersion mechanisms involved in the sample. The asymmetric peak, which is similar to other ferroelectrics (Lu *et al* 1992a, b; Kim and Kim 2000), can be explained using the equivalent circuits: CQR for low temperature and (CQR)(CR) for high temperature, as shown in figure 5 (inset), where $C = A(j\omega)^{m-1}$ and $Q = A(j\omega)^{n-1}$ are Jonscher's (1983) universal capacitances. The frequency dependence of a.c. complex impedance can be expressed as (Lu *et al* 1992a, b),

$$Z^* = \frac{R_o}{1 + (j\omega/\omega_1)^m + (j\omega/\omega_2)^n},$$

where $\omega_1 = 2\pi f_1$ and $\omega_2 = 2\pi f_2$ are the first and second characteristic angular frequencies, respectively. An excellent agreement between experimental and calculated values for both real and imaginary parts of impedance is observed from nonlinear curve fitting as shown in figure 7 using the formula (Lu *et al* 1992a, b)

$$Z'' = \frac{R_o}{(\omega/\omega_1)^m + (\omega/\omega_2)^{-n}}.$$

The variation of fitting parameters (m and n) with temperature is shown in figure 7(a). This plot (m vs temperature) confirms that, it is close to unity and temperature-independent. On the other hand, the value of n is less than one
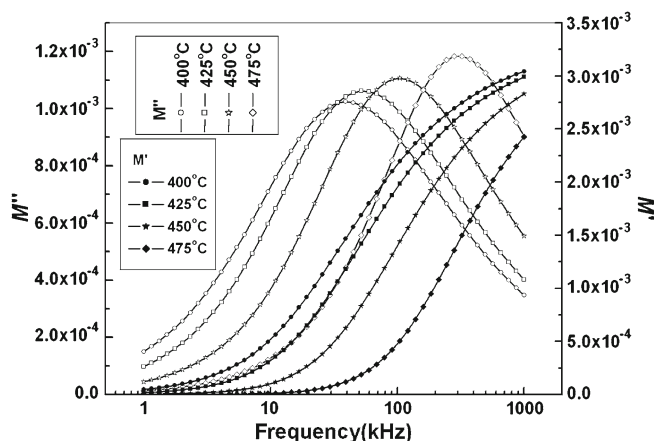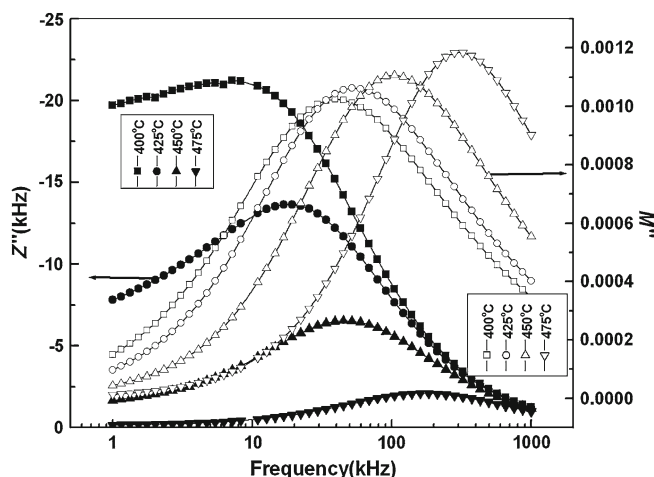
and is temperature-dependent. In the ferroelectric state, the value of n decreases and it attains minimum at T_c, and subsequently increases with temperature. The minimum value of n at (T_c) once again can be explained by restoring force between charge carriers and lattice (Lu *et al* 1992a, b). The above variation in the value of n can also be understood by the theory given by Dissado and Hill (1979, 1980). According to them, exponent n characterizes the magnitude of correlation in a single dipole reorientation. The unity value corresponds to fully correlated transition and zero value corresponds to fully uncorrelated transition. In our experiment, n tends to be minimum at T_c, suggesting a strongly uncorrelated reorientation of the charge carrier polarization at transition point.

The temperature dependence of each of the characteristic frequencies, ($f_1 = \omega_1/2\pi$) and ($f_2 = \omega_2/2\pi$) is shown in figure 7(b) (inset). At transition point, both the frequencies attain minimum. This implies closer the material approaches. Curie point, longer the time required to relax after perturbation (Lu *et al* 1992a, b).

3.4b *Modulus analysis*: The electrical modulus analysis is very useful to detect electrode polarization, grain boundary conduction effect, bulk properties of electrical conductivity and relaxation time (Hodge *et al* 1975; Das *et al* 2007a, b). Figure 8 shows variations of M' and M'' with frequency at selected temperatures. The value of M' approaches zero at low frequency. The monotonic dispersion with rise in frequency may be due to the presence of conduction phenomenon and short range mobility of charge carriers. This implies the lack of restoring force for the flow of charge under the influence of steady electric field (Macedo *et al* 1972). M''_{max} peak shifts to higher frequency side. This nature of dielectric relaxation suggests that the hopping mechanism of charge carriers dominates intrinsically in thermally-activated process. Asymmetric broadening of the

Figure 8. Variation of M' and M'' with frequency at various temperatures of LPLWTN.
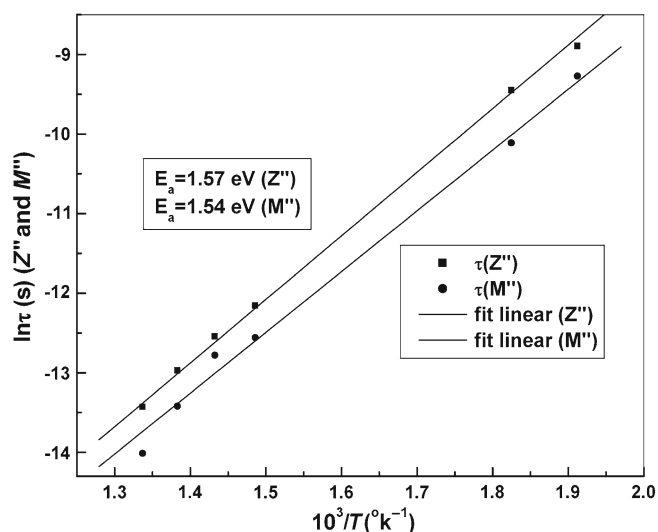

Figure 9. Variation of Z'' and M'' with frequency at different temperatures of LPLWTN.

peak indicates spread of relaxation with different time constants, which suggests non-Debye type (Macdonald 1984).

The impedance (Z'') and modulus (M'') spectroscopy plots are shown in figure 9. The combined plot of Z'' and M'' as a function of frequency is used to detect the presence of smallest capacitance and largest resistance as suggested by Sinclair and West (1989). This will help, whether relaxation process is short range or long range motion of charge carriers. If the process is short range, peaks of Z'' and M'' occur at different frequencies otherwise for long range movement of charge carrier peaks occur at same frequencies (Nobre and Lanfredi 2003; Pradhan *et al* 2009). In the studied compound, there is mismatch of peaks at different temperatures which again suggests short range motion of charge carrier and departure from ideal Debye-like behaviour (Nobre and Lanfredi 2003).

Figure 10 shows variation of relaxation time (τ_r) (calculated from Z'' and M'' vs frequency plot) with reciprocal of absolute temperature which follows Arrhenius

Figure 10. Variation of $\ln\tau$ (calculated from Z'' and M'' with the reciprocal of absolute temperature ($10^3/T$) of LPLWTN.
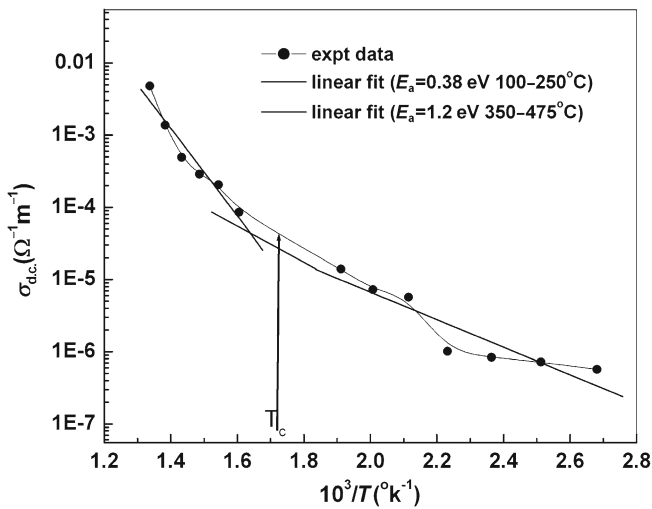
behaviour ($\tau_r = \tau_o \exp(-E_a/k_BT)$), where symbols have their usual meanings. The calculated activation energy (1·57 eV) from Z'' spectra represents localized conduction (i.e. dielectric relaxation), whereas the activation energy (1·54 eV) calculated from modulus spectra represents non-localized conduction (i.e. long range conduction) (Pradhan *et al* 2009). Nearly same activation energy calculated from both the spectra suggests that charge carrier taking part in both localized and non-localized conductions are similar (Raymond *et al* 2005). In comparison to our previous reports like Na₂Pb₂Sm₂W₂Ti₄Nb₄O₃₀ (Das *et al* 2007a, b, c), Na₂Pb₂Nd₂W₂Ti₄Nb₄O₃₀ (Das *et al* 2008), Na₂Pb₂R₂W₂Ti₄V₄O₃₀ (R = Gd, Eu) (Das *et al* 2007a, b, c), ferroelectric and related properties of Li₂Pb₂Pr₂W₂Ti₄Nb₄O₃₀ (LPPWTN) (Parida *et al* 2012) relaxation time of present work decreases and hence, the decrease in the activation energy.

3.5 *D.C. conductivity*

D.C. electrical conductivity of the material is calculated by a simple equation:

$$\sigma_{d.c.} = \frac{t}{AR_b},$$

where t and A represent the thickness and area of the sample, respectively. Figure 11 shows temperature dependence of d.c. conductivity of the material. It is observed that the value of $\sigma_{d.c.}$ increases with rise in temperature which supports NTCR behaviour of the sample. The plot follows Arrhenius relation $\sigma_{d.c.} = \sigma_0 e^{(-E_a/k_BT)}$ (Das *et al* 2007c), where symbols have their usual meanings. The calculated activation energy (E_a) of the sample in the low temperature region (100–250 °C) is 0·38 eV, whereas it is 1·2 eV in the high temperature region (250–475 °C). It is found that these values of E_a are different from the values calculated from the relaxation

Figure 11. Variation of d.c. conductivity with temperature of LPLWTN.

Figure 12. Variation of a.c. conductivity as a function of frequency (conductivity spectrum) at different temperatures.
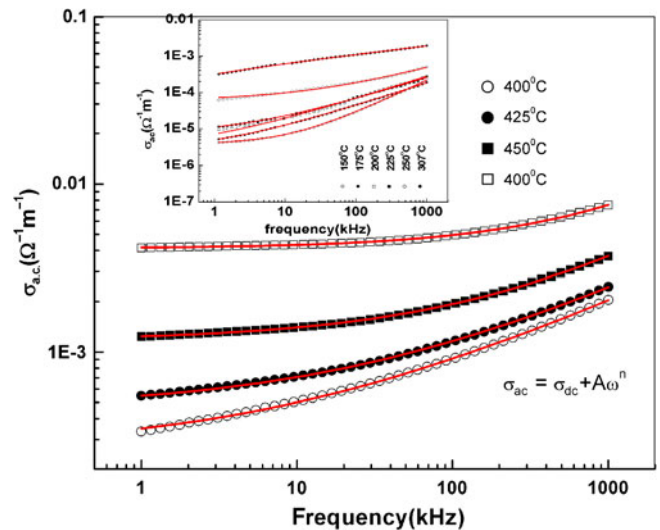
time plots. Because of the difference in the charge carriers, they are responsible for conduction and relaxation processes (Das *et al* 2008). Also, difference in the value of activation energy in low and high temperature regions supports the hopping-type conduction mechanism (Das *et al* 2007a, b, c).

3.6 *A.C. conductivity*

A.C. electrical conductivity ($\sigma_{a.c.}$) is calculated using the dielectric data and an empirical relation, $\sigma_{a.c.} = \omega \varepsilon_r \varepsilon_0 \tan \delta$, where ε_0 is the permittivity in free space and ω the angular frequency. In order to get better understanding of conduction mechanism in the material, we have to follow Jonscher's universal power law (Jonscher 1977): $\sigma_T(\omega) = \sigma(0) + \sigma_1(\omega) = \sigma_0 + A\omega^n \cdot \sigma(0)$ is the frequency independent term giving d.c. conductivity, whereas $\sigma_1(\omega)$ is the purely dispersive component of a.c. conductivity. The exponent n can have a value between zero and one. The value of n is temperature and material dependent but frequency independent.

Figure 12 shows variation of $\sigma_{a.c.}$ in the material with frequency at different temperatures. The conductivity plots show some dispersion in the low frequency region. The value of $\sigma_{a.c.}$ increases with rise in frequency, but it is nearly independent in the low frequency region. The extrapolation of this part towards lower frequency side gives $\sigma_{d.c.}$. The increasing trend of $\sigma_{a.c.}$ with rise in frequency (at low frequency region) may be attributed to the disordering of cations between neighbouring sites and presence of space charge. But in the high frequency region, curves approach to each other and thus coincide.
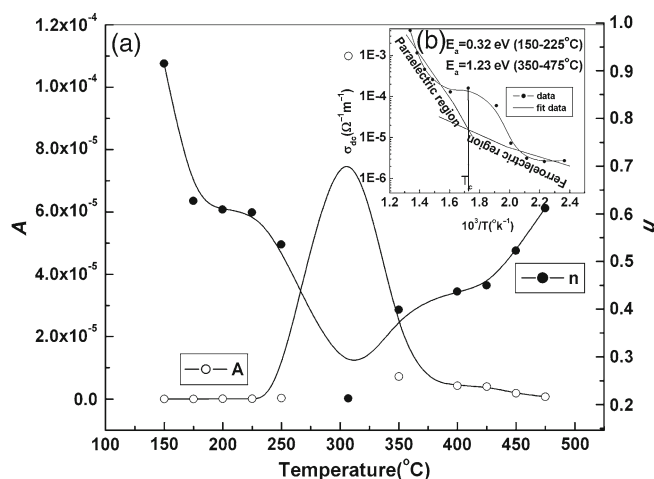
The nature of conductivity plots reveals that the curves exhibit low frequency dispersion phenomena obeying Jonscher's power law. The origin of the frequency dependence of conductivity lies in the relaxation phenomena arising due to mobile charge carriers (Jonscher 1977). When a mobile charge carrier hops to a new site from its original position,

it remains in a state of displacement between two potential energy minima. Also, the conduction behaviour of the materials obeys the power law; $\sigma(\omega) \propto \omega^n$ with a slope change governed by n in the low temperature region. Value of n less than unity ($n < 1$) signifies that the hopping motion involves in the translational motion with a sudden hopping. Whereas $n > 1$ means that the motion involves localized hopping without the species leaving the neighbourhood. The frequency at which change in slope takes place is known as hopping frequency of the polarons (ω_p) and is temperature dependent. The low and high frequency dispersion has been attributed to a.c. conductivity. Whereas, the frequency independent plateau region corresponds to d.c. conductivity. From nonlinear fitting, it is found that the motion of charge carriers are translational because of small value of n (< 1) (Funke 1993). The d.c. conductivity increases with rise in temperature (as expected) in the given material. The values of d.c. conductivity, A and n have been compared in figure 13(a, b). Figure 13(b) shows variation of d.c. conductivity with inverse of absolute temperature, which shows similar trend as seen in figure 11. The calculated activation energy is found to be 1·23 eV in the high temperature region, which is consistent with that of calculated value from figure 11. Again low and high temperature linear fit intersect at a point which is very close to T_c, suggesting the existence of ferroelectric–paraelectric phase transition. Figure 13(a) shows variation of A and n as a function of temperature. It has been observed that the value of n decreases with rise in temperature and attains minimum at T_c, then it increases with further increase in temperature. At the same time, the values of pre-exponential factor A have reverse trend and attain maximum at T_c. The value of exponent n represents degree of interaction between mobile ions and the lattices surround them (Lu *et al* 1992a, b). With rise in temperature, there is increase in interaction among the charge carriers and lattices which lead to decrease in the value

Figure 13. (**a**, **b**) Variation of d.c. conductivity, *A* and *n* as a function of temperature.

of *n*. The minimum value of *n* at T_c implies a strong interaction among charge carriers and lattices. The pre-exponential factor *A* determines the strength of polarizibility. The maximum value of *A* at T_c implies higher polarizibility, i.e. maximum dielectric constant (Pradhan *et al* 2011). In comparison to our previous work on Na$_2$Pb$_2$Sm$_2$W$_2$Ti$_4$Nb$_4$O$_{30}$ (Das *et al* 2007a, b, c), Na$_2$Pb$_2$Nd$_2$W$_2$Ti$_4$Nb$_4$O$_{30}$ (Das *et al* 2008), Na$_2$Pb$_2$R$_2$W$_2$Ti$_4$V$_4$O$_{30}$ (R= Gd, Eu) (Das *et al* 2007a, b, c), ferroelectric and related properties of Li$_2$Pb$_2$Pr$_2$W$_2$Ti$_4$Nb$_4$O$_{30}$ (LPPWTN) (Parida *et al* 2012), both d.c. and a.c. conductivities of the present work increase.

4. Conclusions

The polycrystalline LPLWTN has been synthesized in single phase orthorhombic crystal structure at room temperature. From SEM study, it has been concluded that the grain growth was completed during sintering. The observation of dielectric anomaly at 307 °C and hysteresis loops below this temperature confirmed ferroelectric properties of the material. Detailed studies of electrical or impedance properties of the materials of TB bronze family indicate that the material has (i) conduction due to bulk up to temperature 400 °C, (ii) NTCR-type behaviour and (iii) temperature dependent relaxation phenomena. The impedance spectrum has been used to estimate the contributions of bulk and grain boundary in electrical conductivity. The activation energy of the sample estimated from (i) the conductivity pattern, (ii) relaxation time, (iii) modulus pattern and (iv) fitting model, is almost similar. This indicates that same type of charge carriers are available for both the electrical conduction and electrical relaxation phenomena in the sample. The activation energy due to grain boundary effect confirmed the possible existence of electrical conduction of the material due to mobility of oxygen ions. Modulus analysis exhibits non-exponential type of conductivity relaxation in the material.

References

Behera B, Nayak P and Choudhury R N P 2005 *Mater. Lett.* **59** 3489

Behera B, Nayak P and Choudhary R N P 2007 *J. Alloys Compd.* **436** 226

Behera B, Nayak P and Choudhary R N P 2008 *Mater. Res. Bull.* **43** 401

Bouziane M, Taibi M and Boukhari A 2011 *Mater. Chem. Phys.* **129** 673

Choudhary R N P, Sanigrahi S R and Singh A K 1999 *Bull. Mater. Sci.* **22** 975

Cullity B D 1978 *Elements of X-ray diffraction* (Addison Wesley: Boston, USA)

Das P R, Choudhary R N P and Samantray B K 2007a *Mater. Chem. Phys.* **101** 228

Das P R, Choudhary R N P and Samantray B K 2007b *J. Phys. Chem. Solids* **68** 516

Das P R, Chakraborty P K, Behera B and Choudhary R N P 2007c *Phys.* **B395** 98

Das P R, Choudhary R N P and Samantray B K 2008 *J. Alloys Compd.* **448** 32

Dissado L A and Hill R M 1979 *Nature* **279** 685

Dissado L A and Hill R M 1980 *Philos. Mag.* **B41** 625

Fang L, Zhang H, Huang T H, Yuan R Z and Liu H X 2005 *J. Mater. Sci.* **40** 533

Funke K 1993 *Solid State Chem.* **22** 111

Ganguli P and Jha A K 2011 *Bull. Mater. Sci.* **34** 907

Ganguli P, Devi S and Jha A K 2009 *Ferroelectrics* **381** 111

Goodman G 1953 *J. Am. Ceram. Soc.* **36** 368

Hodge I M, Ingram M D and West A R 1975 *J. Electroanal. Chem. Interfacial Electrochem.* **58** 429

Hornebecq V, Elissalde C, Reau J M and Ravez J 2000 *Ferroelectrics* **238** 57

Jonscher A K 1977 *Nature* **267** 673

Jonscher A K 1983 *Dielectric relaxation in solids* (London: Chelesa Dielectric Press)

Josse M *et al* 2009 *Solid State Sci.* **11** 1118

Kim J S and Kim J N 2000 *Jpn. J. Appl. Phys.* **39** 3502

Kim M S, Lee J H, Kim J J, Lee H Y and Cho S H 2006 *J. Solid State Electro. Chem.* **10** 18

Klug H P and Alexander L E 1974 *X-ray diffraction* (England: Wiley Chester) pp 966–969

Lu Z, Bonnet J P, Ravez J, Reau J M and Hagenmuller P 1992a *Phys. Chem. Solids* **53** 1

Lu Z, Bonnet J P, Ravez J and Hagenmuller P 1992b *Solid State Ionics* **57** 235

Macdonald J R 1984 *Solid State Ionics* **13** 147

Macedo P B, Moynihan C T and Bose R 1972 *Phys. Chem. Glasses* **13** 171

Muktha B, Simon A, Darriet J and Guru Row T N 2006 *Chem. Mater.* **18** 1240

Nobre M A L and Lanfredi S 2003 *J. Appl. Phys.* **93** 5557

Parida B N, Das Piyush R, Padhee R and Choudhary R N P 2012 *J. Phys. Chem. Solids* **73** 713

Pilgrim S M, Sutherland A E and Winzer S R 1990 *J. Am. Ceram. Soc.* **73** 3122

Plocharski J and Wieczoreck W 1988 *Solid State Ionics* **28** 979

Powd E W 1983 *An interactive powder diffraction data interpretation and indexing program*, Ver 2.1, School of Physical Science (Australia: Bedford Park, S.A., Finders University of South Australia) p. 5042

Pradhan D K, Choudhary R N P, Rinaldi C and Katiyar R S 2009 *J. Appl. Phys.* **106** 024102

Pradhan D K, Behera B and Das P R 2011 *J. Mater. Sci.: Mater. Electron.* **23** 779

Ranjan R, Kumar R, Kumar N, Behera B and Choudhury R N P 2011 *J. Alloys Compd.* **509** 6388

Raymond O, Font R, Suaerz-Almodovar N, Portelles J and Siqueiros J M 2005 *J. Appl. Phys.* **97** 084108

Sahoo P S, Panigrahi A, Patri S K and Choudhary R N P 2010 *Bull. Mater. Sci.* **33** 129

Sambasiva Rao K, Murali Krishana P, Madhava Prasad D, Lee J H and Kim J S 2008 *J. Alloys Compd.* **464** 497

Sen S, Choudhary R N P and Pramanik P 2007 *Phys. B* **387** 56

Sinclair D C and West A R 1989 *J. Appl. Phys.* **66** 3850

Smolenskii G A and Agranovskaya A I 1954 *Dokl. Akad. Nauk. SSSR* **97** 237

Suman C K, Prasad K and Choudhary R N P 2006 *J. Mater. Sci.* **41** 369

Wul B and Goldman I M 1945 *C. R. Acad. Sci. URSS* **46** 139